Angewandte Chemie
Eine Zeitschrift der Gesellschaft Deutscher Chemiker

Supporting Information

Mechanically Triggered Hybridization Chain Reaction

Yuxin Duan, Roxanne Glazier, Alisina Bazrafshan, Yuesong Hu, Sk Aysha Rashid, Brian G. Petrich, Yonggang Ke, and Khalid Salaita**

anie_202107660_sm_miscellaneous_information.pdf
anie_202107660_sm_movie_1.avi
anie_202107660_sm_movie_2.avi

SUPPORTING INFORMATION

Table of Contents

Experimental Procedures and materials

1) Materials

Cy3B-NHS ester (PA63101) was purchased from GE Healthcare Life Sciences (Pittsburgh, PA). Atto647N-NHS ester (18373) was purchased from Sigma Aldrich (St. Louis, MO). Cyclo[Arg-Gly-Asp-d-Phe-Lys(PEG-PEG)] (PCI-3696-PI) (cRGD) was acquired from Peptides International (Louisville, KY). Streptavidin (S000-01) was purchased from Rockland-Inc (Pottstown, PA). µ-Slide VI0.4 6-channel slides (80606) and 25 mm x 75 mm glass coverslips (10812) were purchased from Ibidi (Verona, WI). ProPlate® Microtiter (204969) are purchased from Thermo-Fisher Scientific. N-hydroxyl succinimide-5 kDa PEG-biotin (NHS-PEG-biotin, HE041024-5K) was purchased from Biochempeg (Watertown, MA). Sulfo-N-hydroxyl succinimide-acetate (sulfo-NHS-acetate26777) was purchased from Thermo-Fisher (Waltham, MA). (3-Aminopropyl) triethoxysilane (APTES, 440140, 99% purity) was purchased from Sigma-Aldrich, Adenosine 5'-diphosphate (ADP, A2754, 95% purity) was purchased from sigma -Aldrich. All oligonucleotides are listed in Table S1 and purchased from Integrated DNA Technologies (Coralville, IA). All other reagents and materials (unless otherwise stated) were purchased from Sigma-Aldrich and used without purification. All buffers were prepared with 18.2 MΩ nanopure water.

Table S3. List of used oligonucleotides

Name	Sequence (5' to 3')
Unzipping mode Initiator	/5AmMC6/GAG GAG GGC AGC AAA CGG GAA GAG TCT TCC TTT ACG TTT T /3Bio/
Shearing mode Initiator	/5Biosg/ TT/iAmMC6T/ GAG GAG GGC AGC AAA CGG GAA GAG TCT TCC TTT ACG T
BHQ2 Ligand Strand	/5 hexynyl/ ACG TAA AGG AAG ACT CTT CCC GTT TGC TGC CCT CCT C/3BHQ2/
H1	/5AmMC6/CGT AAA GGA AGA CTC TTC CCG TTT GCT GCC CTC CTC GCA TTC TTT CTT GAG GAG GGC AGC AAA CGG GAA GAG
H2	/5AmMC6/GAG GAG GGC AGC AAA CGG GAA GAG TCT TCC TTT ACG CTC TTC CCG TTT GCT GCC CTC CTC AAG AAA GAA TGC
Scramble ssDNA control	/5Hexynyl/CGC ATC TGT GCG GTA TTT CAC /iAmMC6T/TT T/3Bio/

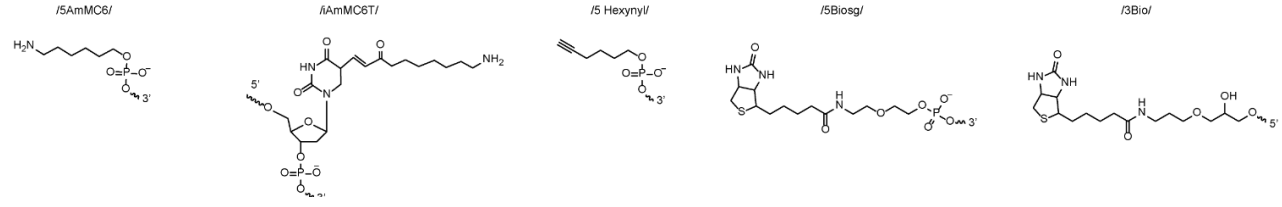

2) Instruments

SUPPORTING INFORMATION

We used two main microscopes for the work. The first was a Nikon Eclipse Ti microscope, operated by Nikon Elements software, using a 1.49 numerical aperture (NA) CFI Apo ×100 objective, perfect focus system, a TIRF laser launch, a Chroma quad cube (ET-405/488/561/640 nm Laser Quad Band) and an RICM (Nikon: 97270) cube for mechano-HCR experiments. The second was an N-STORM Nikon microscope (Ti E motorized inverted microscope body), operated by Nikon Elements software, equipped with an Intensilight epifluorescence source (Nikon), a CFI Apo 100X NA 1.49 objective was used in surface density characterization experiments and a Plan Fluor 10X objective was used to capture brightfield images of NIH/3T3 cells on 96 well plates. Bulk fluorescence measurements were conducted using a Synergy H1 plate reader (Bio-Tek) using fluorescence filter sets. All ultrapure water was obtained from a Barnstead Nanopure water purifying system (Thermo Fisher) that indicated a resistivity of 18.2 MΩ. Nucleic acid purification was performed using a high-performance liquid chromatography (HPLC, Agilent 1100) equipped with a diode array detector. Microvolume absorbance measurements were obtained using a Nanodrop 2000 UV-Vis Spectrophotometer (Thermo Scientific). Mass identification of product was performed with a Matrix-assisted laser desorption/ionization time-of-flight mass spectrometer (MALDI-TOF-MS, Voyager STR). Agarose gels were run with a Mini-Sub Cell GT Horizontal electrophoresis system and imaged with Gel Doc EZ imager (Bio-Rad)

3) Surface Preparation

Mechano-HCR surface preparation method was modified from previously published protocols.[1] Briefly, rectangular glass coverslips (25 x 75 mm, Ibidi) were rinsed with water and sonicated for 20 minutes in water and 20 minutes in 50% ethanol. The glass converslips were then cleaned with piranha solution. The piranha solution was prepared using a 1:3 mixture of H_2O_2 and H_2SO_4. WARNING: Piranha solution becomes very hot upon mixing, and is highly oxidizing and may explode upon contact with organic solvents. Then, slides were washed 6 times in beakers with ultrapure water, followed by 4 successive washes using ethanol. In a separate beaker of ethanol, slides were reacted with 3% v/v APTES at room temperature for 1 h. Coverslips were then washed 6 times with ethanol, baked in oven for 20 minutes at 80 °C. Slides were then reacted with NHS-PEG-biotin (1% w/v) for 1 hr in ultrapure water. Next, slides were washed 3 times with ultrapure water, dried under N_2 gas, and then stored at -30°C for up to 2 weeks before use. At the day of imaging, the 5kDa PEG-biotin surface was adhered onto µ-Slide VI0.4 6-channel ibidi slide or proplate microtiter with adhesive bottom. Wells were then reacted for 1hr with sulfo-NHS-acetate (1% w/v) in 0.5 M K_2SO_4 and 0.1M $NaHCO_3$ (pH 9) to consume any unreacted amines on the surface. To further reduce non-specific DNA binding during the imaging, the wells were then washed with 1XPBS and passivated with 5% v/v Tween 20 in T50 buffer for 30 min. The wells were then washed with 1XPBS and incubated with 50µg/ml streptavidin for one hour. The wells were then washed with 1XPBS and incubated with 100nM DNA probe solutions for 1 hr. Finally, the wells were washed with cell imaging buffer before imaging.

4) DNA Hybridization

DNA oligonucleotides and DNA hairpins were hybridized at 100 nM in a 0.2 µL PCR tube. DNA was firstly heated to 90°C and then cooled at a rate of 1.3°C per min to 35°C. Hairpin strands were also annealed on the experimental day before use using this same protocol to ensure that the oligos adopt the folded state and hence reduce leakage of HCR polymerization. [2]

5) Oligo dye/ligand coupling and purification

All sequences of DNA strands used in this work are provided in **Supplementary Table 1**. Firstly, 100 nmoles of c(RGDfK(PEG-PEG)) was reacted with ~ 200 nmoles of NHS-azide in DMSO overnight (**Fig. S5**). Product 1 was then purified via reverse phase HPLC using a Grace Alltech C18 column (Solvent A: water + 0.05% TFA, Solvent B: acetonitrile + 0.05% TFA; starting condition: 90% A + 10 % B, 1%/min; Flow rate: 1 mL/min)

Purified product 1 was ligated to the BHQ_2 ligand strand via 1,3-dipolar cycloaddition click reaction. Briefly, 5 nmoles of alkyne ligand strand was reacted with ~70 nanomoles of product 1. The total reaction volume is 50 µL, composed of 0.1 M sodium ascorbate and 0.1 mM Cu-THPTA for 2h at room temperature. The product was then purified with a P2 size exclusion column, and then purified with reverse phase HPLC using Agilent Advanced oligo column (Solvent A: 0.1M TEAA, Solvent B: acetonitrile; starting condition: 90% A + 10 % B, 0.5%/min gradient B, Flow rate: 0.5 mL/min) (**Fig. S5**).

10 nmole Amine labelled hairpin strands were reacted overnight with a 20x excess of Cy3B-NHS dissolved in 10 µL DMSO. The total volume of the reaction was 100 µL, composed of 1x PBS supplemented with 0.1M $NaHCO_3$. Then P2 size exclusion gel was used to remove unreacted dye. The product was then purified by reverse phase HPLC using Agilent Advanced oligo column (Solvent A: 0.1M TEAA, Solvent B: acetonitrile; starting condition: 90% A + 10 % B, 1%/min gradient B, Flow rate: 0.5 mL/min) to purify products 4 and 5 (**Fig. S5**).

The retention times of all products and starting reagents are shown in **Fig. S5**. Concentrations of purified oligonucleotide conjugates were determined by measuring their A260 absorption value on a Nanodrop 2000 UV-Vis Spectrophotometer (Thermo Scientific). MALDI-TOF mass spectrometry was performed on high performance MALDI time-of-flight mass spectrometer (Voyager STR). The matrix for all experiments was freshly prepared by dissolving excess 3-hydroxypicolinic acid (3-HPA) in the matrix solvent (50% MeCN/H_2O, 1% TFA, 10% of 50 mg/mL ammonium citrate).

Table S4. MALDI-TOF analysis of modified oligonucleotides for this study

Sample	Calculated mass	m/z found (MALDI-TOF)	Error
Atto 647N Unzipping mode Initiator	14467	14882	2%
Atto 647N Shearing mode Initiator	13788	13372	3%
cRGDfk-BHQ2 strand	12783	12840	0.4%
Cy3B-H1	23376	23411	0.1%
Cy3B-H2	22986	23357	1%

6) Solution based hybridization chain reaction (HCR) and agarose gel electrophoresis,

HCR reactions shown in **Figure 2b** and **Figure S1** were performed at room temperature for 1.5 h with each hairpin at 1 μM concentration. DNA initiator was diluted to different concentrations (30, 3, 1.5, 0.3, and 0.03 μM) in ultrapure water. The initiator was added to H1 and H2 mixture solution to bring the final initiator concentration to 10, 1, 0.5, 0.1, and 0.01 μM. When initiator was absent (lane 7, **Figure 2b**), ultrapure water was added to bring the reaction volume to 30 μL. After incubation, HCR samples were mixed with 6 μL of 6× gel loading buffer (15% (w/v) Ficoll (Type 400; Pharmacia) in H_2O) and loaded into a native 2% agarose gel, prepared with 1× TBE buffer and stained with ethidium bromide. The gel was run at 60 V for 90 min at 4°C and imaged using a gel imager (Bio-Rad).

7) Mouse platelet handling

Blood from C57Bl/6J mice was collected by cardiac puncture, anticoagulated with acid citrate dextrose, added to equal volumes modified Tyrode's buffer (140mM NaCl, 2.7mM KCl, 0.4mM NaH_2PO_4, 10mM $NaHCO_3$, 5mM Dextrose, 10mM HEPES) containing 3U apyrase and centrifuged at 200xg for 5min. The platelet fraction was removed and to it added 1U apyrase and 1uM prostaglandin E1. Platelets were centrifuged at 700xg for 5min and resuspended in Walsh buffer (137mM NaCl, 2.7mM KCl, 1mM $MgCl_2$, 3.3mM NaH_2PO_4, 20mM HEPES, pH 7.4, 0.1% glucose, 0.1% bovine serum albumin) at a concentration of $1x10^9$ platelets/ml.[3] Experimental procedures were approved by the Emory University Institutional Animal Care and Use Committee.

8) Cell culture

Mouse embryonic fibroblasts (MEF) and NIH/3T3 fibroblasts were cultured according to ATCC guidelines. Briefly, cells were cultured in DMEM supplemented with 10% fetal bovine serum (v/v) and penicillin/streptomycin. Cells were passaged every 2-3 days as required.

9) Mechanically-triggered hybridization chain reaction

Mechanically-triggered Hybridization chain reaction was performed on the prepared biotin surface as described in the surface preparation section. First, hybridized TGT probes (prehybridized initiator and ligand strands) were incubated on biotin surface in 1x PBS buffer for 1h. The wells were washed with cell imaging buffer (DMEM with 1% FBS for 3T3 cells and Tyrodes buffer for platelets). Then, cells were added onto the cRGDfK-labelled duplex surfaces for 1h to promote cell adhesion. Subsequently, H1 and H2 solution were mixed in imaging buffer and added to the wells (96 well plates) or channels(ibidi slides) to initiate the HCR reaction with mechanically exposed initiator. After 2h of incubation, wells and channels were gently washed with 1ml cell imaging medium to remove non-reacted hairpins to decrease background. Afterwards, surfaces with exposed initiators and HCR polymers were imaged directly with fluorescence microscopy for high resolution characterization and quantification. Bulk fluorescence intensities on 96 well plates were measured with a Bio-Tek® Synergy H1 plate reader (Ex/Em = 540/590 nm for HCR channel and Ex/Em = 620/680 nm duplex rupture channel).

10) Dose-dependent inhibition of integrin mediated tension

For dose-dependent inhibition of integrin experiments, the cell density of 3T3 fibroblasts was first characterized with a hemocytometer. Same number of 3T3 cells (20000) in cell culture medium were then incubated with different concentrations of inhibitor in the cell culture incubator for 30 minutes before plating onto 96 well plates. Afterwards, cells were incubated for 1h to promote cell adhesion. Then the mechano-HCR protocol was followed to achieve amplification and quantification.

For platelet mechano-HCR measurements, mouse platelets were purified and incubated at room temperature for at least 30 min before beginning experiments. Platelets were then treated with drugs for 30 min before seeding onto 96 well-plate. 2 μM ADP was added to promote cell adhesion. Then platelets were incubated at room temperature for 1h. The same mechano-HCR protocols were followed to achieve amplification and quantification for platelets as is the case for 3T3 cells.

11) Microscopy imaging

For mechano-HCR experiments, Images were acquired on a Nikon Eclipse Ti microscope, operated by Nikon Elements software, a 1.49 NA CFI Apo 100x objective, perfect focus system, and a total internal reflection fluorescence (TIRF) laser launch with 488 nm (10 mW), 561 nm (50 mW), and 638 nm (20 mW). A reflection interference contrast microscopy (RICM) (Nikon: 97270) cube and a Chroma quad cube (ET-405/488/561/640 nm Laser Quad Band) were used for imaging. Imaging was performed on 96 well plates and glass coverslips using DMEM as cell imaging media for 3T3 cells and Tyrode's buffer for platelets. All imaging data was acquired at room temperature.

For surface characterization experiments, a Nikon Eclipse Ti microscope equipped with Evolve electron multiplying charge coupled device (Photometrics), an Intensilight epifluorescence source (Nikon), a CFI Apo 100X NA 1.49 objective was used. All of the imaging was performed using reflection interference contrast microscopy (RICM) and the Chroma filter cubes: TRITC, Cy5. Note that a Nikon Plan Fluor 10X objective was used to capture brightfield images of NIH/3T3 cells on 96 well plates shown in **Figure 3B**.

12) Determination of DNA surface density

We adapted a reported surface density quantification assay,[4] which converts the raw fluorescence intensity of a surface to the density of fluorescent molecules. In this assay, lipid membranes are used as fluorescence standards, because of their known density of fluorescent species. In this calibration, the intensity of labeled oligonucleotides and small unilamellar vesicles (SUVs) in solution are compared to determine the F factor, which relates molecular brightness of two fluors. The concentration of oligonucleotide probes on mechano-HCR surfaces is calcuatled using the F factor, along with a fluorescence calibration curve generated by imaging supported lipid bilayers (SLBs) of known dye density.

Small unilamellar vesicles (SUV) were made from 1,2-dioleoyl-sn-glycero-3-phosphocholine (DOPC) (850375C, Avanti Polar Lipids) and 1,2-dioleoyl-sn-glycero-3-phosphoethanolamine-N-(Cyanine 5) (Cy5-PE, 810335, Avanti Polar Lipids). First, lipids were added to a round-bottom flask containing chloroform. The mixture contained either 100 mol % DOPC or 99.9 mol% DOPC and 0.1 mol % Cy5 PE. Lipids were placed under rotary evaporation followed by an ultra-high-purity nitrogen stream to remove chrloroform. SUVs were formed by sonicating the lipids in nanopure water, with a lipid concentration of 2 mg/mL. To generate monodisperse unilamellar vesicles SUVs were freeze-thawed 3x and were extruded 10x. Extrusion was performed with a 10 mL LIPEX Extruder (Transferra Nanosciences, Inc.) containing a 0.08 µm polycarbonate filter (WHA110604, Whatman) and a drain disc (WHA230600, Whatman). The working concentration of Cy5-PE in the sample was experimentally calculated using a Thermo Scientific Nanodrop 2000c spectrophotometer.

To relate dye brightness, the brightness of known concentrations of labeled oligonucleotides and SUVs were measured in solution. Glass was passivated with 1% BSA in PBS for 35 min. Good quality measurements was assessed by looking at the ratio of concentration to intensity, as deviations can indicate nonspecific adsorption. The F factor labeled oligonucleotide and SUV brightness was defined as, $F = I_{\mathrm{Atto647N}-DNA} / I_{\mathrm{Cy5}-DHPE}$.

SUVs were also used to make supported lipid bilayers (SLBs) in glass-bottom 96-well plates (265300, Nunc). The glass was treated with a 2.6 M NaOH etch and was thoroughly washed with water followed by 1x PBS. To create a fluorescence calibration curve, SLBs with varying fluorophore concentration were prepared by adding mixtures of labeled and unlabeled SUVs in known stoichiometries. Excess SUVs were rinsed using water and PBS. The intensity of the SLBs was measured using epifluorescence microscopy. Using the known lipid footprint[4] (DOPC lipid footprint in supported bilayers of 0.72 nm^2), the resulting curve was used to relate absolute density of fluorophores to arbitrary fluorescence units. These data were then used to convert the intensity of initiator surfaces incubated with varying concentrations of initiators to initiators per micron-squared. The equation of this conversion is shown in the **Figure S3**, $DNA\ density = 2 \times intensity \div (F \times slope)$.

Results and discussions

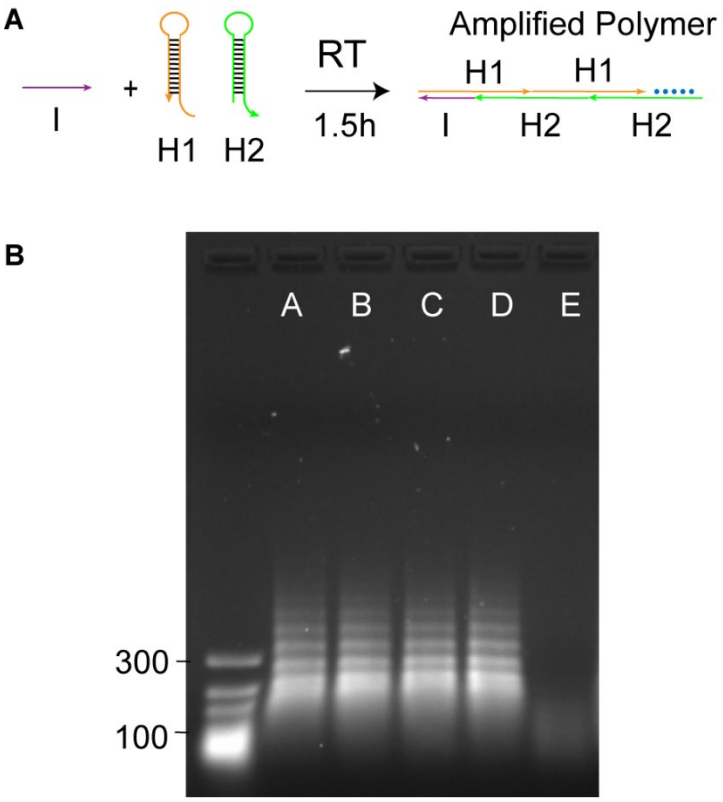

Figure S1. Agarose gels used to validate HCR polymers in different buffers. (A) Schematic shows the protocol used to initiate HCR. (B) Agarose gel electrophoresis of HCR products in different buffers. H1, H2 and initiator are at 1 μM concentration. Left lane: ultra-low range DNA ladders. A: HCR in 1xPBS, B: HCR in DMEM buffer, C: HCR in Hanks' buffer, D: HCR in Tyrode's buffer. E: H1 in 1xPBS buffer without I and H2.

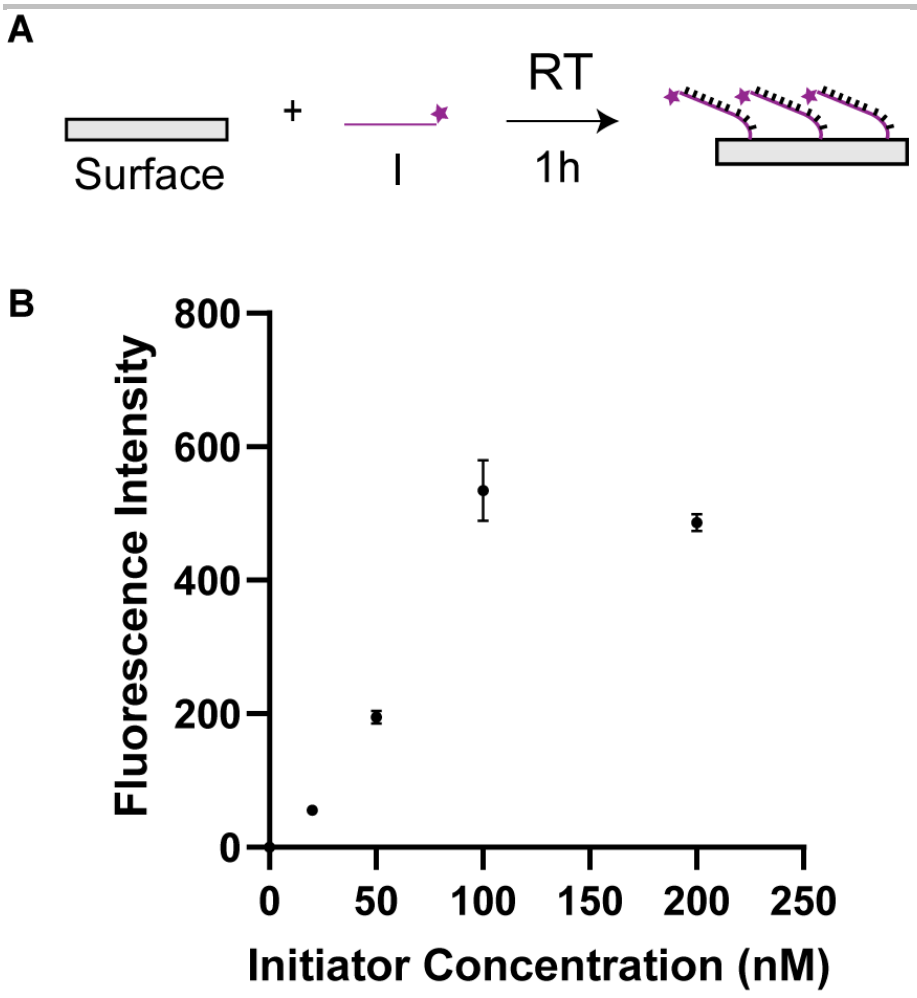

Figure S2: Characterization of surface coverage with different initiator concentration when incubated on prepared surface. (A) Schematic of immobilization of biotin labeled initiator on streptavidin surface (B) plots of fluorescence intensity of initiator on surface with initiator concentration when incubated on streptavidin surface (6 measurements per concentration per experiment, n = 3 independent experiments). Error bars represent the standard deviation from three independent experiments.

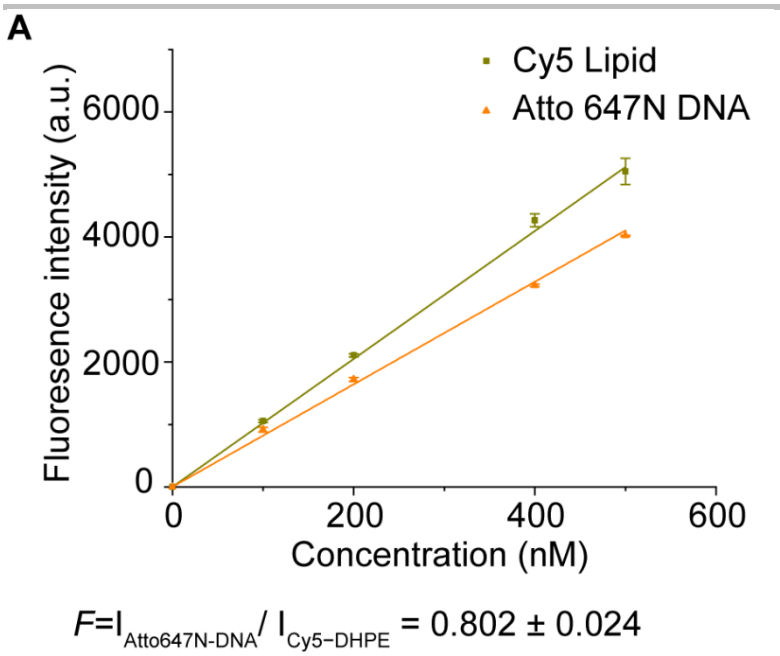

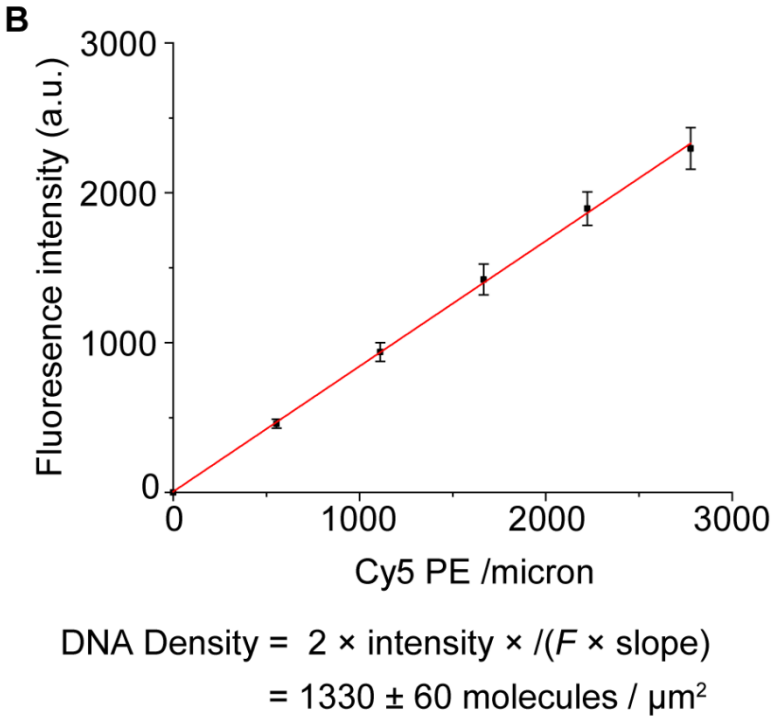

Figure S3. Quantifying DNA probe density on surface. (A) Plot of fluorescence intensity versus concentration for Cy5-tagged phospholipid vesicles and Atto647N-DNA. These measurements were performed in solution. Error bars represent the standard deviation from n = 3 independent preparations where each preparation was measured 5 times. F factor was calculated as the ratio of Atto647N to Cy5 fluorescence. Error calculated from the propagated standard deviation of Atto647N-DNA/Cy5-DHPE measurements. (B) Plot of fluorescence intensity versus Cy5 phospholipid per micron within the SLB (6 measurements from $n = 3$ independent experiments. This plot was used to convert the fluorescence measurements of Atto 647N-DNA initiator surface into molecular density. Probe density was 1330 ± 60 probes per square micron (Error calculated from propagated SEM).

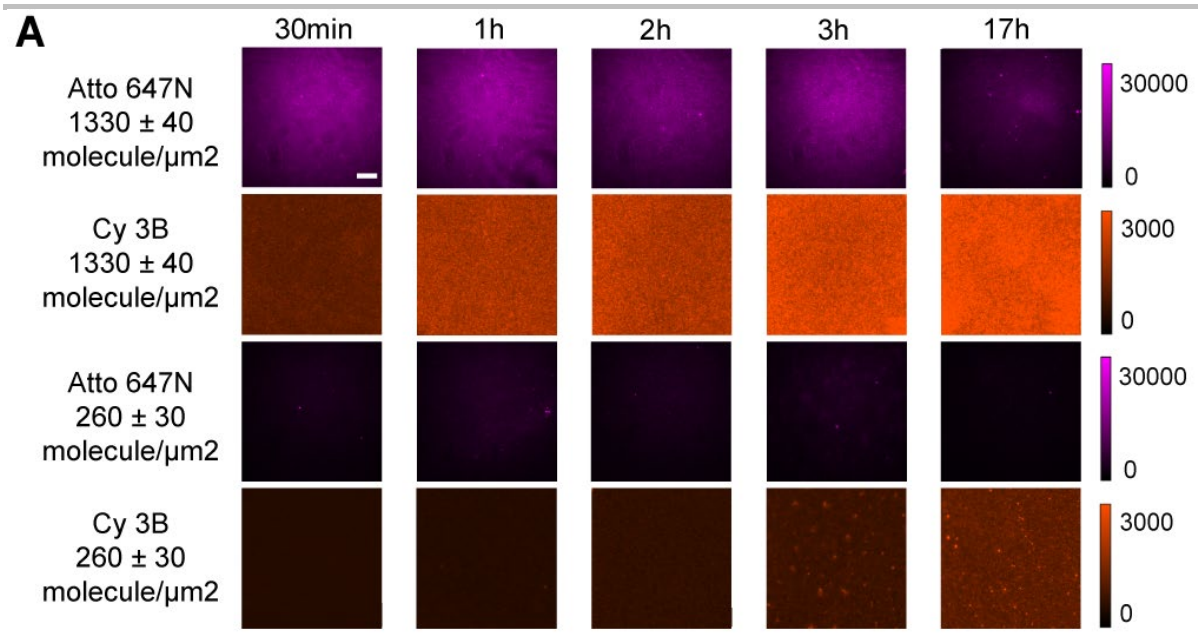

Figure S4. Representative Fluorescence images showing surface density and surface HCR activity at different time point. The high-density initiator surfaces (top two rows) were generated by incubating the surface with 100 nM bulk concentration of DNA for 1 hr. The lower density surfaces (lower two rows) were created by incubating the substrates with 20 nM biotinylated DNA for 1 hr. Note that the magenta (Atto647N) signal is constant or is reduced as a function of time, since this signal only reports the density of initiator. In contrast, the Cy3B signal grows as a function of time due to the progress of the HCR. This data was used to generate the plot in figure 2D. Scale bar = 10 µm

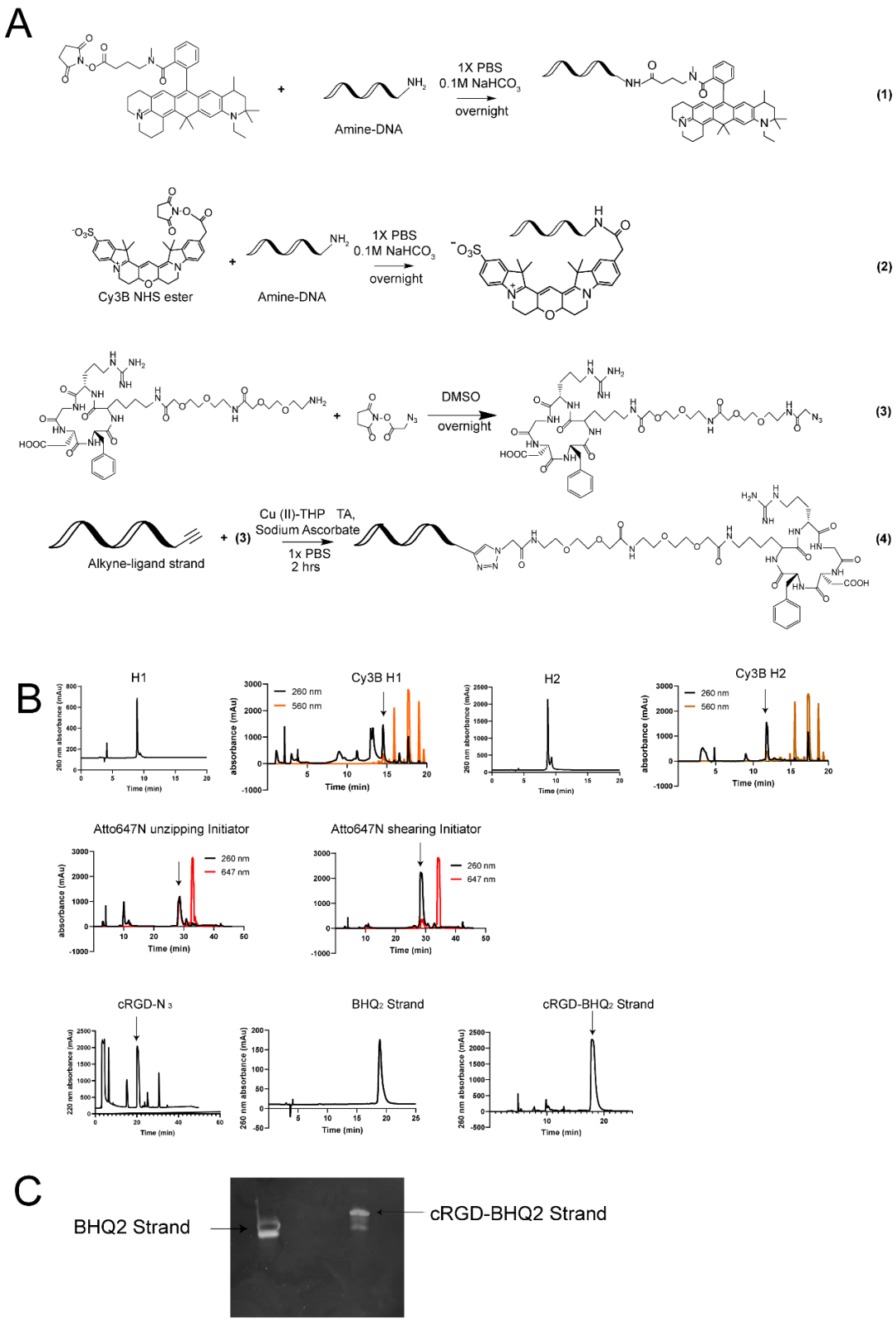

Figure S5: Characterization of modified oligonucleotides: A) Chemical structures and reactions of oligonucleotides, dye NHS esters and cRGDfk peptides. (B) HPLC traces of reaction products. Reactions were monitored using 260 nm absorbance unless otherwise noted. Arrows indicate the peaks associated with the products and that were isolated for mass spectrometry analysis. (C) PAGE gel electrophoresis of BHQ2 strand starting material and the cRGDfk modified BHQ_2 strand product.

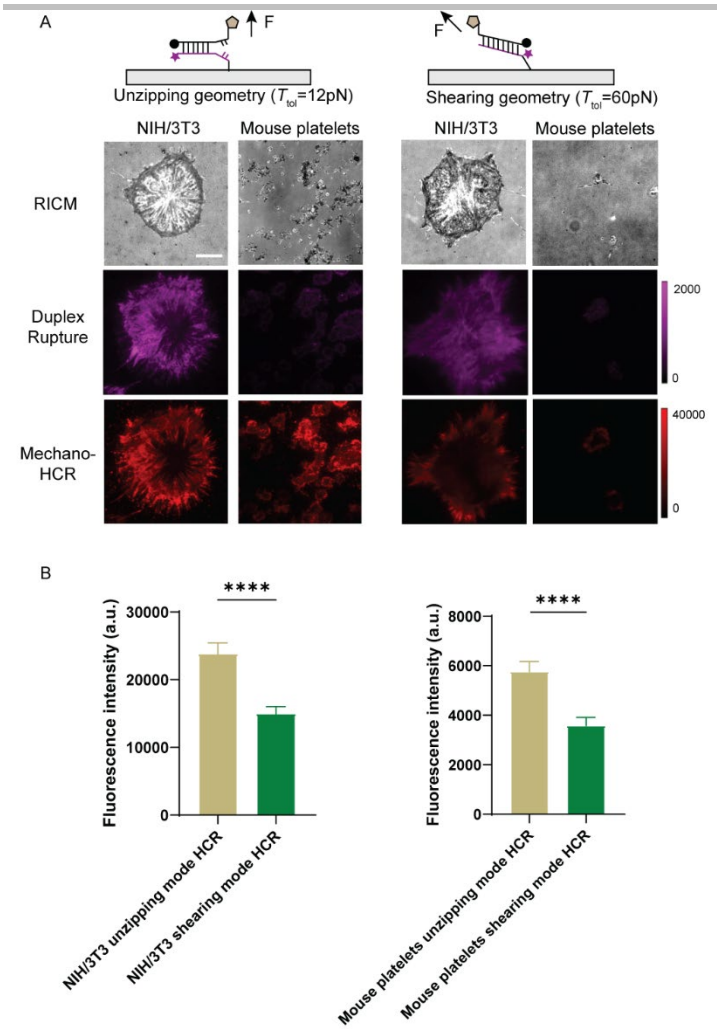

Figure S6. Comparison of mechano-HCR triggered by unzipping and shearing duplex rupture. (A) Schematic of DNA duplexes in the shearing and unzipping geometries with cryptic initiator used to study integrin-mediated forces (top). Representative RICM and fluorescence images of cells cultured on unzipping (T_{tol}=12 pN) and shearing (T_{tol}= 60 pN) surfaces after HCR amplification. Scale bar = 10 μm. The magenta color is emission from Atto647N that was used to tag the initiator (bottom strand), while the red channel shows the Cy3B emission that is due to H1 and H2 accumulation following HCR. The intensity bar next to each fluorescence image shows the absolute signal intensity for each image. (B) Bar graph quantifying the HCR fluorescence intensity for NIH/3T3 cells and mouse platelets on unzipping (T_{tol}= 12 pN) and shearing (T_{tol}= 60 pN) surfaces. The error bar represents S.E.M. from 36 cells in n=3 independent experiments (**** $p < 0.0001$, student t-test).

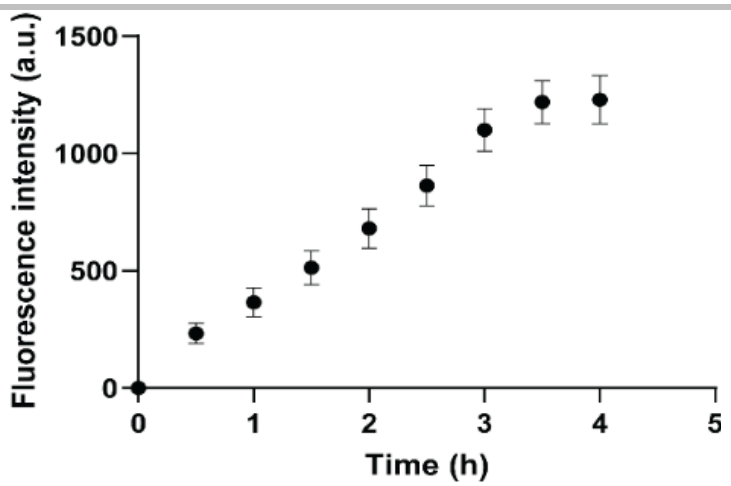

Figure S7. Time-resolved mechano-HCR using TIRF microscopy. Plot of time-dependent fluorescence intensity of mechano-HCR under cells measured with total internal reflection fluorescence (TIRF). Error bars represent S.E.M. obtained from three independent experiments. The intensity at each time point was determined by averaging the fluorescence signal from 12 cells in each experiment. The background intensity was quantified from regions outside of the cell at t = 0 hr, and this signal was subtracted from the measurements. The mechano-HCR experiment was performed as described in the methods section. NIH/3T3 cells were incubated on the surface for 1h before hairpin monomers were added. Representative real-time change of fluorescence for one cell is shown in **Supplementary movie 1**.

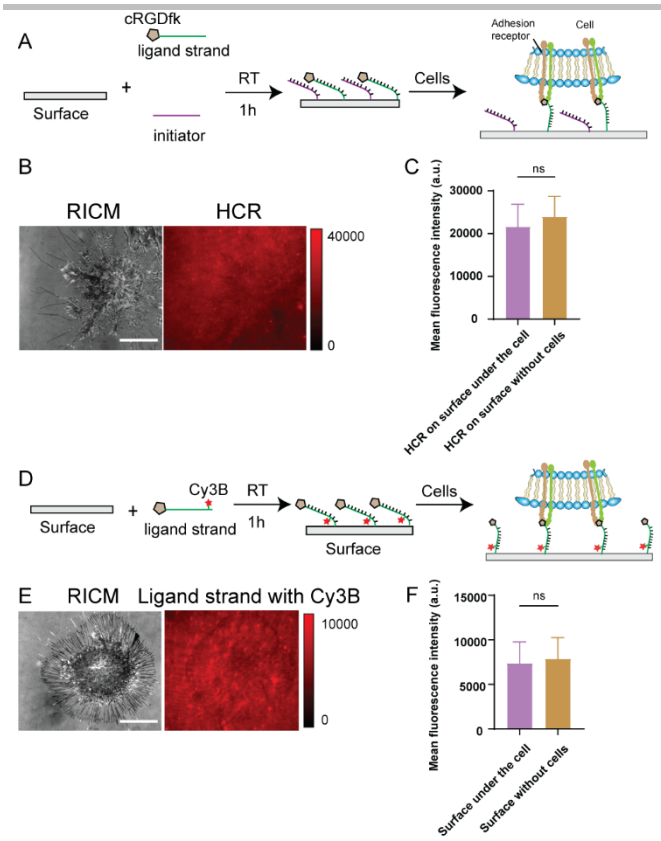

Figure S8. Controls showing that cell-surface junction does not significantly hinder mechano-HCR. (A) Schematic showing control surfaces that present a binary mixture of two oligonucleotides. The first was modified with the cRGD peptide and the second oligo functioned as the initiator for HCR. The surface was prepared by mixing a 1:1 ratio of these two oligonucleotides with total concentration = 100 nM. To test the mechano-HCR assay, we seeded 20,000 cells on the surface for 1h before hairpins were added to drive HCR amplification. (B) Representative RICM and fluorescence (Cy3B) images showing the signal due to HCR reaction. The HCR was allowed to proceed for 2 hr. Scale bar = 10 μm. (C) Plot of HCR fluorescence intensity in areas under the cell and outside cells. Error bar represents the standard deviation from n = 20 cells. The HCR signal is slightly reduced under the cell but the decrease is not statistically significant (based on student's *t* test). (D) To test if nucleases contribute to the loss of fluorescence under the cells, we designed control surface that presented a monolayer of ssDNA that is Cy3B and cRGD modified. Surfaces were prepared by incubating with a 100 nM solution of the nucleic acid. Following our standard procedures, 20,000 cells were seeded on the surface for 1h prior to imaging. (B) Representative RICM and fluorescence (Cy3B) images of this control experiment. Scale bar = 10 μm. Note that the brightness of this surface is lower here because there was no HCR amplification performed in this control. (F) Plot of fluorescence intensity of Cy3B in areas under the cell and outside the cell attachment regions. Error bar represents SD from n = 20 cells. Consistent with the plots in (C), the fluorescence signal under the cells is slightly reduced but is not significantly different from that of the regions outside of the cell.

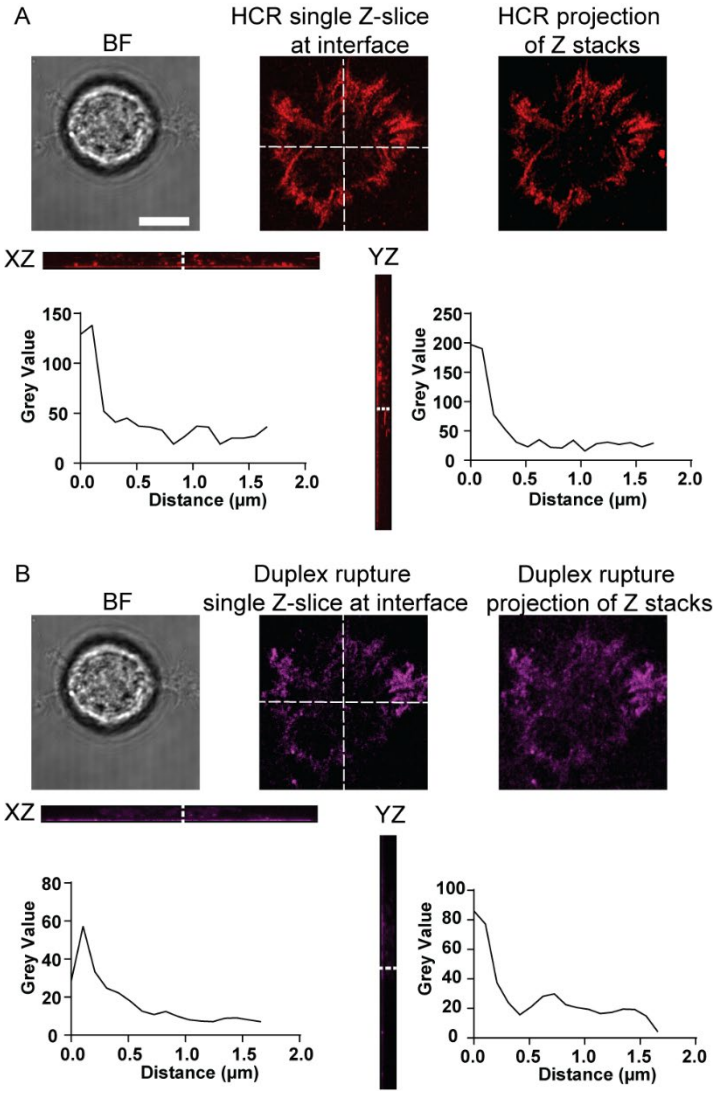

Figure S9. Confocal Z-stack images showing mechano-HCR signal is primarily localized to the cell-surface junction. (A) Representative brightfield, fluorescence image showing a single z slice of the HCR signal, and projection of *z* stack of images on the *x-y* plane. The single z-slice was collected at the cell-surface junction. Dashed white lines indicate the location of line scans in the *x-z* and the *y-z* projection. Scale bar = 10 μm. Plots show the fluorescence intensity as a function of distance for the line scans indicated on the image. The data indicates that the HCR product is confined to a diffraction limited plane along the substrate surface. **(B)** Representative brightfield, fluorescence image showing a single z slice of the duplex rupture signal, and projection of *z* stack of images on the *x-y* plane. The single z-slice was collected at the cell-surface junction. Dashed white lines indicate the location of line scans in the *x-z* and the *y-z* projection. Scale bar = 10 μm. Plots show the fluorescence intensity as a function of distance for the line scans indicated on the image. The data indicates that the duplex rupture signal is localized to the substrate surface as expected.

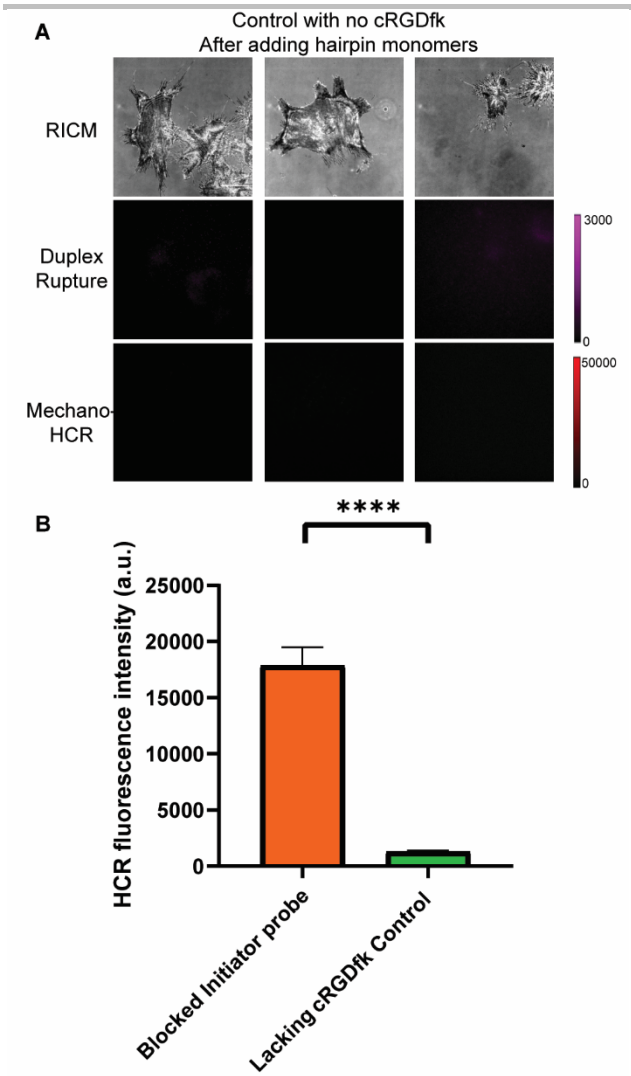

Figure S10. Characterization of nonspecific HCR signal using cRGDfk lacking oligonucleotide controls. (A) Representative RICM, Atto647N and Cy3B images for cells incubated on DNA duplex surface lacking cRGDfk ligand after the H1 and H2 monomers were added for 2h. Scale bar = 10 μm. (B) Bar graph showing the fluorescence intensity of mechano-HCR chips measured using fluorescence microscopy. The orange bar shows the +cRGDfK (positive control group) while the green bar shows identical substrates that were modified with -cRGDfK (negative control group). Error bar representative S.E.M. of 8 measurements from $n = 3$ independent experiments (****$p < 0.0001$, student *t*-test).

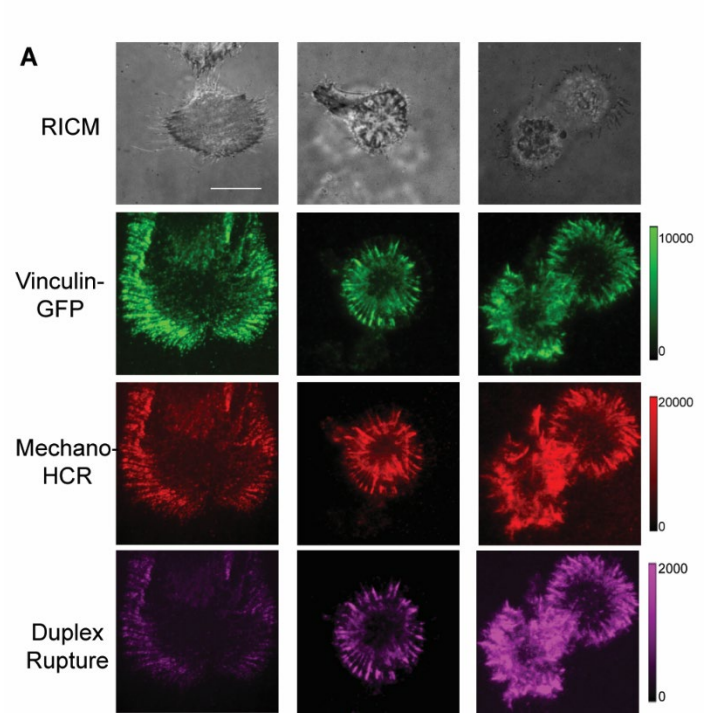

Figure S11. Colocalization between focal adhesion and mechano-HCR with vinculin-GFP MEF cells. (A) Representative RICM, FITC, Cy3B and Atto647N channel microscope images of mechano-HCR performed using vinculin-GFP expressing mouse embryonic fibroblasts. Fluorescence images show colocalization between focal adhesions and the mechano-HCR amplified signal with a measured Pearson's correlation coefficient of 0.81 ± 0.05 (*n* = 15 cells from 3 independent experiments). Scale bar = 12 μm.

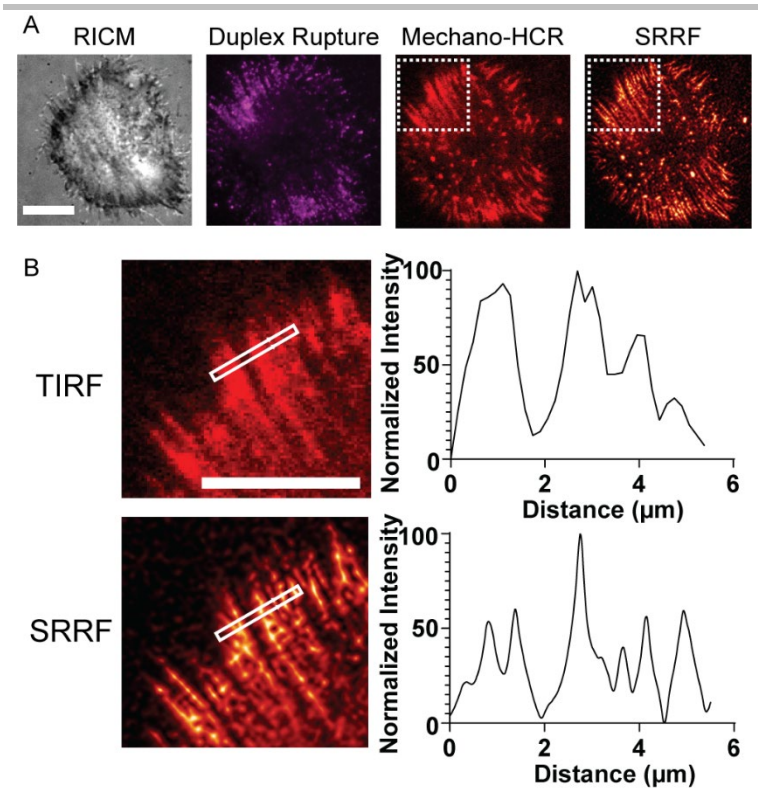

Figure S12. SRRF super resolution imaging showing improved resolution of mechano-HCR. (A) Representative RICM and fluorescence images of NIH/3T3 cells imaged using super-resolution radial fluctuations (SRRF) experiments. The image shown in magenta represents the Atto647N channel used to tag the initiator (bottom strand) while the red channel shows the Cy3B emission from H1 and H2 accumulation following HCR. Scale bars = 10 um. White dashed box indicates the region of interest that is highlighted in B. Super resolved imaging via SRRF was performed on a 20 second time lapse series of 1000 frames with 20 ms exposure time in the mechano-HCR channel. In SRRF analysis, ring radius was set as 0.5; ring magnification was 10 and the axes in ring were set to 8. (B) Zoom in of the ROI from (A) and plot of line scan showing improved resolution using SRRF compared to conventional TIRF image. Scale bar = 10 μm. This data shows that the mechano-HCR signal is amenable to super resolution imaging methods. SRRF HCR images are representative of 3 independent experiments.

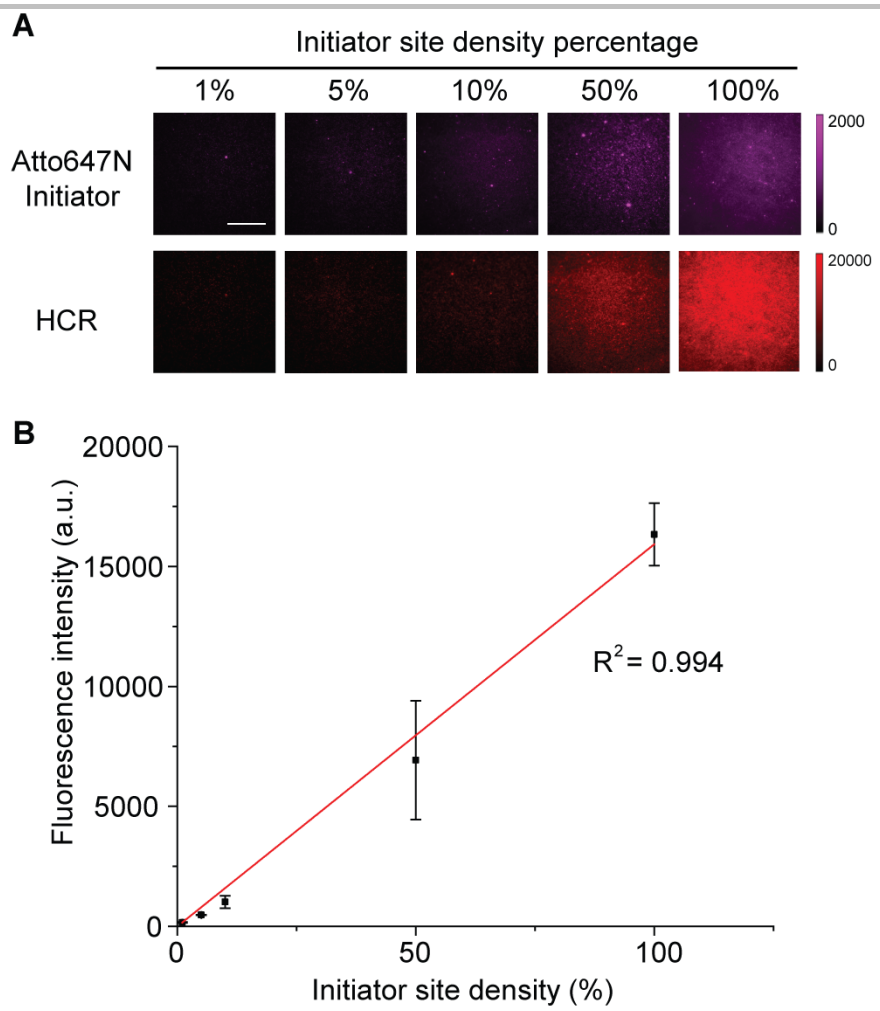

Figure S13. Quantification of HCR intensity as a function of initiator site density. (A) Representative fluorescence images showing Atto647N intensity and Cy3B intensity as a function of initiator site density following 2 hr HCR. Scale bar = 10 μm. To tune the initiator surface density, we mixed the initiator with a scrambled initiator that was also biotinylated. The total oligonucleotide concentration was maintained at 100 nM for all measurements. (B) Plot of HCR fluorescence intensity versus initiator site density. Linear regression showed an R^2 = 0.994 which indicates a linear relationship at the conditions tested. Error bar represents SD from 8 measurements from *n* = 3 experiments.

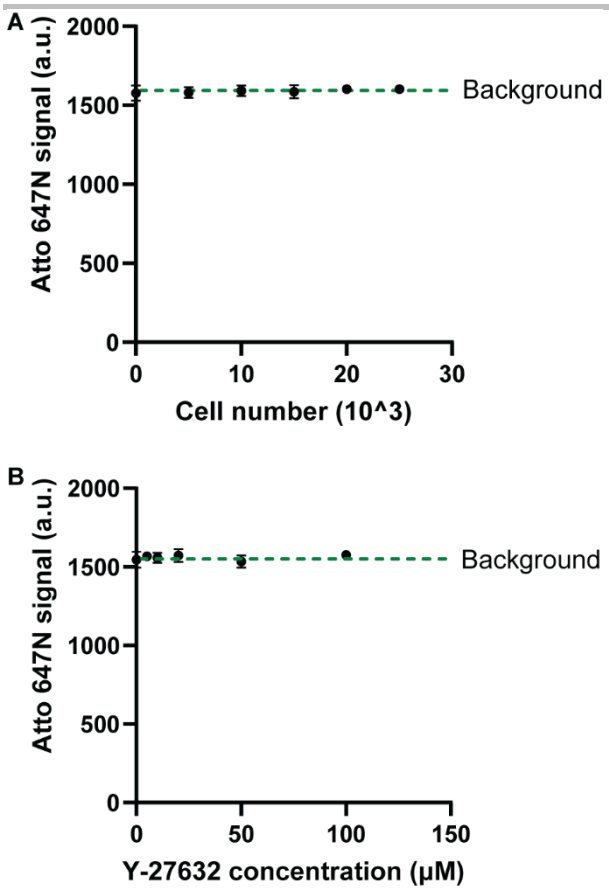

Figure S14. Controls showing that plate reader fails to detect duplex rupture signal. (A) Plot of DNA duplex unzipping fluorescence as a function of cell plating number (NIH/3T3 cells). (B) Plot of DNA unzipping fluorescence intensity as a function of Y-27632 dose for 20,000 cells plated per well. For both plots, the data was collected using a plate reader measuring the emission of the Atto647N reporter >2 hrs after cell seeding. Note that the same plate reader and settings were used to detect the mechano-HCR signal shown in **Figure 3** & **4** in the main text. Error bar represents S.E.M. from n = 3 independent experiments. Dashed green line represents the background intensity generated from a surface that lacked the DNA probes. The background was calculated by averaging the signal from three control surfaces lacking DNA.

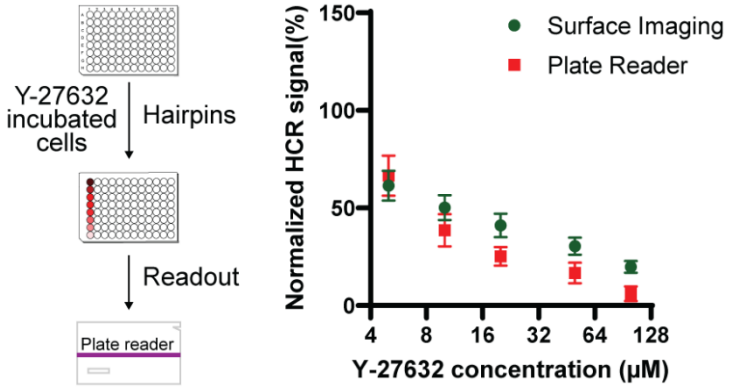

Figure S15. Comparison between microscopy and plate reader HCR signal for NIH/3T3 cells. Schematic and plot of plate reader measured mechano-HCR signal as a function of Y-27632 concentration. Drug was incubated for 30 min prior to seeding. Error bar represents S.E.M. from 3 independent experiments. The values were normalized to the signal obtained from the 20,000 cells/well samples without drug treatment. All measurements were background subtracted using negative control wells lacking cells. The red points are the mechano-HCR signals measured using a plate reader while the green points were obtained using a fluorescence microscope from individual platelets.

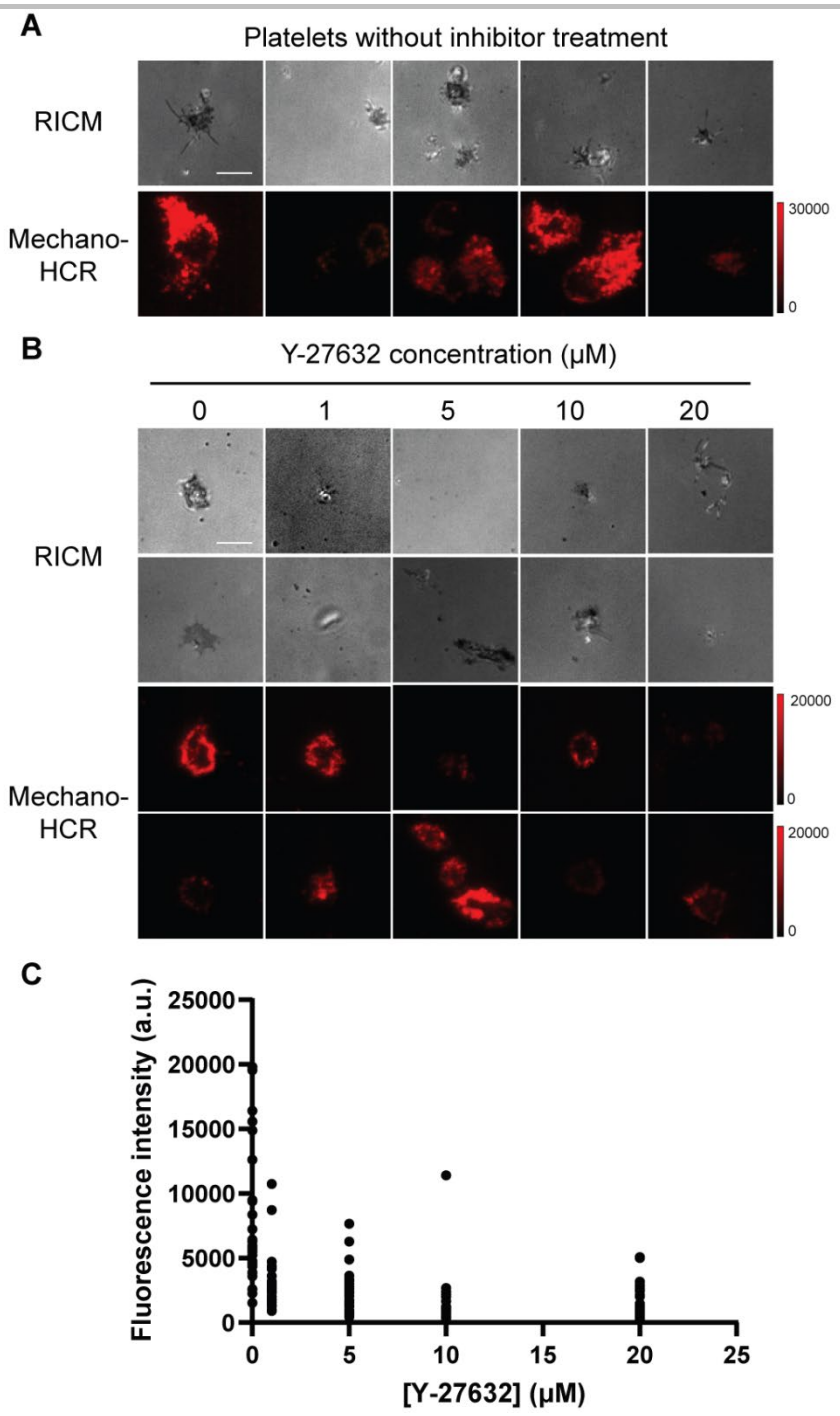

Figure S16. Examples showing cell to cell heterogeneity for mouse platelets mechano-HCR signal. (A) Representative RICM and fluorescence images showing the variability between individual platelets that were isolated from the same animals and cultured in the same well under identical conditions. Scale bar = 5 μm. (B) Representative RICM and fluorescence images showing cell to cell variability of individual platelet mechano-HCR signal when compared between different wells. Scale bar = 5 μm. Mouse platelets were incubated with different doses of the ROCK inhibitor for 30 min and then added to 96 well plates for 1 hr and then imaged. (C) Plot of mechano-HCR fluorescence intensity of individual platelets obtained from fluorescence images as a function of Y-27632 concentration, *n*=30 cells from three independent animal samples.

Table S1. Representative literature investigating force spectroscopy of DNA

Title	Year	Journal	Notes
Dynamic force spectroscopy of single DNA molecules[5]	1999	Proc. Natl. Acad. Sci. USA	AFM force-spectroscopy to study separation of DNA duplex
Force-induced melting of a short DNA double helix[6]	2001	Eur. Biophys. J.	AFM measurements of force-induced melting of short DNA duplexes
Measurement of the phase diagram of DNA unzipping in the temperature-force plane[7]	2004	Phys. Rev. Lett.	Magnetic tweezer study of DNA unzipping at different temperatures
Single-molecule cut-and-paste surface assembly[8]	2008	Science	AFM based transfer of DNA strands across a surface
Unraveling the structure of DNA during overstretching by using multicolor, single-molecule fluorescence imaging[9]	2009	Proc. Natl. Acad. Sci. USA	Combined optical tweezers/fluorescence microscopy of DNA meltings under force
Single-molecule derivation of salt dependent base-pair free energies in DNA[10]	2010	Proc. Natl. Acad. Sci. USA	Optical tweezer and modeling of mechanical unzipping of single DNA molecules
Maximum pull out force on DNA hybrids[11]	2001	C. R. Acad. Sci., Ser. IV: Phys.	Modeling of forces on DNA hybrids
Shear unzipping of DNA[12]	2009	J. Phys. Chem. B	Modeling of unzipping of DNA duplexes
Force-induced rupture of a DNA duplex: from fundamentals to force sensors[13]	2015	ACS Nano	Modeling of force-induced rupture of DNA duplexes with course-grained oxDNA

Table S2. Representative literature describing the use of DNA-based tension sensors to characterize cell forces.

Title	Year	Journal	Notes
DNA-based digital tension probes reveal integrin forces during early cell adhesion[14]	2014	Nat. Commun.	First report of a DNA hairpin tension sensor
DNA-based nanoparticle tension sensors reveal that T-cell receptors transmit defined pN forces to their antigens for enhanced fidelity[15]	2016	Proc. Natl. Acad. Sci. USA	T cells transmit pN forces to their TCRs to regulate immune response
Notch-Jagged complex structure implicates a catch bond in tuning ligand sensitivity[16]	2017	Science	DNA probes to study Notch mechanosensor model
B cell antigen extraction is regulated by physical properties of antigen-presenting cells[17]	2017	J. Cell Biol.	DNA probes to study B cell receptors mechanobiology
Platelet integrins exhibit anisotropic mechanosensing and harness piconewton forces to mediate platelet aggregation[18]	2018	Proc. Natl. Acad. Sci. USA	DNA probes used to study platelet activation and shows that 12-56 pN integrin tension is associated with the earliest steps of platelet activation.
Real-time measurement of molecular tension during cell adhesion and migration using multiplexed differential analysis of tension gauge tethers[19]	2019	ACS Biomater. Sci. Eng.	DNA duplex rupture probes to study fibroblast cell forces
EGFR activation attenuates the mechanical threshold for integrin tension and focal adhesion formation[20]	2020	J. Cell Sci.	DNA duplex probes used to study how EGFR regulates integrin tension and organization of focal adhesions
Live-cell super-resolved PAINT imaging of piconewton cellular traction force[21]	2020	Nat. Methods	DNA tension probes imaged using DNA-PAINT technique

SUPPORTING INFORMATION

Table S5. Literature reported IC_{50} for drugs used in our work

Inhibitors	Target	Measuring approach	IC_{50}	Reference
Y-27632	*Fibroblast*	*Kinase Essay in vitro*	*~5 μM*	*Mitchison et al.*[22]
Y-27632	Fibroblast	Morphology assays (Focus formation)	10 μM (Full inhibation concentration)	Treisman et al. [23]
Y-27632	*Platelets*	*Shape change*	*~1.1 μM*	*Kunapuli et al.*[24]
Epitifibatide	*Platelets*	*Shear induced Adhesion*	*5781 nM*	*Feuerstein et al.*[25]
Epitifibatide	Platelets	ADP induced aggregation	0.66 μM	*Kleiman et al*[26]
Aspirin	*Platelets*	*AA induced aggregation*	*41.2 μM*	*Osawa et al.*[27]
Aspirin	Platelets	AA induced aggregation	24.3 μM	*Sorensen et al.*[28]
Aspirin	COX-1	Enzyme immunoassay	3.57 μM	*Galdo e al .* [29]

*Note that the entries denoted in italic text indicates the literature IC_{50} values that we compare against the mechano-IC_{50} values we measured in this work. These were selected from amongst the various reported values because the cell type and protocols best matched our approaches.

References

[1] Y. Liu, L. Blanchfield, V. P.-Y. Ma, R. Andargachew, K. Galior, Z. Liu, B. Evavold, K. Salaita, *Proc. Natl. Acad. Sci. U.S.A.* **2016**, *113*, 5610-5615.
[2] R. M. Dirks, N. A. Pierce, *Proc. Natl. Acad. Sci. U.S.A.* **2004**, *101*, 15275-15278.
[3] N. Prévost, H. Kato, L. Bodin, S. J. Shattil, *Methods Enzymol.* **2007**, *426*, 103-115.
[4] W. J. Galush, J. A. Nye, J. T. Groves, *Biophys J.* **2008**, *95*, 2512-2519.
[5] T. Strunz, K. Oroszlan, R. Schäfer, H.-J. Güntherodt, *Proc. Natl. Acad. Sci. U.S.A.* **1999**, *96*, 11277-11282.
[6] L. H. Pope, M. C. Davies, C. A. Laughton, C. J. Roberts, S. J. B. Tendler, P. M. Williams, *Eur. Biophys. J.* **2001**, *30*, 53-62.
[7] C. Danilowicz, Y. Kafri, R. S. Conroy, V. W. Coljee, J. Weeks, M. Prentiss, *Phys. Rev. Lett.* **2004**, *93*, 078101.
[8] S. K. Kufer, E. M. Puchner, H. Gumpp, T. Liedl, H. E. Gaub, *Science* **2008**, *319*, 594-596.
[9] J. van Mameren, P. Gross, G. Farge, P. Hooijman, M. Modesti, M. Falkenberg, G. J. L. Wuite, E. J. G. Peterman, *Proc. Natl. Acad. Sci. U.S.A.* **2009**, *106*, 18231-18236.
[10] J. M. Huguet, C. V. Bizarro, N. Forns, S. B. Smith, C. Bustamante, F. Ritort, *Proc. Natl. Acad. Sci. U.S.A.* **2010**, *107*, 15431-15436.
[11] P.-G. de Gennes, *C. R. Acad. Sci., Ser. IV: Phys.* **2001**, *2*, 1505-1508.
[12] B. Chakrabarti, D. R. Nelson, *J. Phys. Chem. B* **2009**, *113*, 3831-3836.
[13] M. Mosayebi, A. A. Louis, J. P. K. Doye, T. E. Ouldridge, *ACS Nano* **2015**, *9*, 11993-12003.
[14] Y. Zhang, C. Ge, C. Zhu, K. Salaita, *Nat. Commun.* 2014, 5, 5167.
[14] Z. Liu, Y. Liu, Y. Chang, H. R. Seyf, A. Henry, A. L. Mattheyses, K. Yehl, Y. Zhang, Z. Huang, K. Salaita, *Nat. Methods* **2016**, *13*, 143-146.
[15] V. C. Luca, B. C. Kim, C. Ge, S. Kakuda, D. Wu, M. Roein-Peikar, R. S. Haltiwanger, C. Zhu, T. Ha, K. C. Garcia, *Science* **2017**, *355*, 1320-1324.
[16] K. M. Spillane, P. Tolar, *J. Cell Biol.* **2017**, *216*, 217-230.
[17] Y. Zhang, Y. Qiu, A. T. Blanchard, Y. Chang, J. M. Brockman, V. P.-Y. Ma, W. A. Lam, K. Salaita, *Proc. Natl. Acad. Sci. U.S.A.* **2018**, *115*, 325-330.
[18] M. H. Jo, W. T. Cottle, T. Ha, *ACS Biomater. Sci. Eng.* **2019**, *5*, 3856-3863.
[19] T. C. Rao, V. P.-Y. Ma, A. Blanchard, T. M. Urner, S. Grandhi, K. Salaita, A. L. Mattheyses, *J. Cell Sci.* **2020**, *133*.
[20] J. M. Brockman, H. Su, A. T. Blanchard, Y. Duan, T. Meyer, M. E. Quach, R. Glazier, A. Bazrafshan, R. L. Bender, A. V. Kellner, H. Ogasawara, R. Ma, F. Schueder, B. G. Petrich, R. Jungmann, R. Li, A. L. Mattheyses, Y. Ke, K. Salaita, *Nat. Methods* **2020**, *17*, 1018-1024.
[21] J. C. Yarrow, G. Totsukawa, G. T. Charras, T. J. Mitchison, *Chem. Biol.* **2005**, *12*, 385-395.
[22] E. Sahai, T. Ishizaki, S. Narumiya, R. Treisman, *Current Biol.* **1999**, *9*, 136-145.
[23] B. Z. Paul, J. L. Daniel, S. P. Kunapuli, *J. Biol. Chem.* **1999**, *274*, 28293-28300.
[24] X. Wang, R. T. Dorsam, A. Lauver, H. Wang, F. A. Barbera, S. Gibbs, D. Varon, N. Savion, S. M. Friedman, G. Z. Feuerstein, *J. Pharmacol. Exp. Ther.* **2002**, *303*, 1114-1120.
[25] B. E. Tardiff, L. K. Jennings, R. A. Harrington, D. Gretler, R. F. Potthoff, D. A. Vorchheimer, P. R. Eisenberg, A. M. Lincoff, M. Labinaz, D. M. Joseph, M. F. McDougal, N. S. Kleiman, *Circulation* **2001**, *104*, 399-405.
[26] M. ABE, Y. OZAWA, Y. UDA, Y. MORIMITSU, Y. NAKAMURA, T. OSAWA, *Biosci. Biotechnol. Biochem.* **2006**, *70*, 2494-2500.
[27] P. Fontana, P. Alberts, K. S. Sakariassen, H. Bounameaux, J. P. Meyer, A. Santana Sorensen, *J. Thromb. Haemostasis* **2011**, *9*, 2109-2111.
[28] F. J. Blanco, R. Guitian, J. Moreno, F. J. de Toro, F. Galdo, *J. Rheumatol.* **1999**, *26*, 1366-1373.

Author Contributions

Y.D. Investigation:Lead; Data curation: Lead; Formal analysis: Lead; Methodology: Lead; Validation: Lead; Writing - Original Draft: Lead; Writing - Review & Editing: Lead;
R.G. Investigation: Supporting; Data curation: Supporting; Validation: Supporting; Writing - Review & Editing: Supporting
A.B. Data curation: Supporting; Writing - Review & Editing: Supporting
Y.H. Investigation: Supporting; Validation: Supporting; Writing - Review & Editing: Supporting
R.A. Validation: Supporting
B.P. Investigation: Supporting; Writing - Review & Editing: Supporting
Y.K. Funding acquisition: Lead; Investigation: Supporting; Project administration: Lead; Supervision: Lead; Writing - Original Draft: Lead; Writing - Review & Editing: Lead.
K.S. Funding acquisition: Lead; Investigation: Supporting; Project administration: Lead; Supervision: Lead; writing - Original Draft: Lead; Writing - Review & Editing: Lead.